DOI: 10.1002/ ((please add manuscript number))

Article type: Full Paper

Green Synthesis of Low Dimensional Aluminum Oxide Hydroxide and Oxide Using Liquid Metal Reaction Media: Ultra-High Flux Membranes

Ali Zavabeti, Bao Yue Zhang, Isabela A. de Castro, Jian Zhen Ou, Benjamin J Carey, Md Mohiuddin, Robi Datta, Chenglong Xu, Adrian P. Mouritz, Christopher F. McConville, Anthony P. O'Mullane, Torben Daeneke, and Kourosh Kalantar-zadeh**

Ali Zavabeti, Bao Yue Zhang, Dr. Isabela A. de Castro, Dr. Jian Zhen Ou, Dr. Benjamin J Carey, Md Mohiuddin, Robi Datta, Dr. Chenglong Xu, Prof. Adrian P. Mouritz, Dr. Torben Daeneke, and Prof. Kourosh Kalantar-zadeh

School of Engineering, RMIT University, Melbourne, VIC 3001, Australia

E-mail: kourosh.kalantar@rmit.edu.au and torben.daeneke@rmit.edu.au

Dr. Benjamin J Carey

Institute of Physics and Center for Nanotechnology, University of Münster, Münster, Germany

Prof. Christopher F. McConville

School of Science, RMIT University, Melbourne, VIC 3001, Australia

Assoc. Prof. Anthony P. O'Mullane

School of Chemistry, Physics and Mechanical Engineering, Queensland University of Technology (QUT), Brisbane, QLD 4001, Australia

Prof. Kourosh Kalantar-zadeh

School of Chemical Engineering, University of New South Wales (UNSW), Sydney, NSW 2052, Australia

Keywords: liquid metals, galinstan, low-dimensional, membranes, boehmite

Liquid metal reaction media provides exciting new avenues for synthesizing low dimensional materials. Here the synthesis of atomically thin sheets and nanofibers of boehmite (γ-AlOOH) and their transformation into cubic alumina (γ-Al_2O_3) *via* annealing is explored. The sheets are as thin as one orthorhombic boehmite unit cell. The addition of aluminum into a room temperature alloy of gallium, followed by exposing the melt to either liquid water or water vapor, allows growing either two-dimensional sheets or one-dimensional fibers, respectively. The isolated oxide hydroxides feature large surface areas, with the sheet-morphologies also showing a high Young's modulus. The method is green, since the liquid metal solvent can be fully reused. The ultrathin boehmite sheets are found suitable for the development of free-standing membrane filters that enable excellent separation of heavy metal ions and oil from aqueous solutions at extraordinary filtrate flux. The developed liquid metal-based synthesis process offers a sustainable, green and rapid method for synthesizing nano-morphologies of metal oxides which are challenging to obtain by conventional

methods. The process is both sustainable and scalable and may be explored for the creation of other types of metal oxide compounds.

1. Introduction

Gallium based liquid metal alloys have emerging applications in microfluidics, flexible and stretchable electronics, reconfigurable devices, optics and electrochemically driven actuators.[1] Recently, they have also been featured as an excellent reaction solvent to produce nano-dimensional compounds of metals.[1g, 2] Gallium can be mixed with many transition and post transition metals to produce alloys or liquid/solid metal colloids with a wide range of interesting characteristics.[1g, 3] Galinstan, is one such example, a non-toxic eutectic alloy containing 68.5 wt% Ga, 21.5 wt% In and 10.0 wt% Sn with a freezing point well below 0ºC.[4] Selected metallic elements can be incorporated onto or alloyed into galinstan itself at relatively high concentrations, leading to a vast family of liquid alloys that may be exploited.[2b, 5]

Wide bandgap low dimensional materials feature remarkable properties for applications in electronics, photonics, electrochemistry and many other fields.[6] These materials can also be applied in other important areas such as membrane technologies and the enhancement to mechanical and other properties of polymer-based materials.[7] One such set of wide bandgap metal oxide compounds is the aluminum oxide family that are in high demand for industrial applications and, despite the abundance of aluminum in nature,[8] their environmentally friendly production into one and two dimensional (1D and 2D) morphologies have rarely been reported.

Oxide hydroxide of aluminum (boehmite γ-AlOOH) is the main component of many bauxite minerals[9] and one of the main precursors used for the production of aluminum oxides.[10] It has been described theoretically[11] and shown experimentally [10a, 12] that cubic alumina (γ-Al_2O_3) adopts an orthorhombic γ-AlOOH morphology when de-hydrated. Cubic alumina is of special importance as this crystal phase of aluminum oxide can readily be transformed into other phases of Al_2O_3.[13] Therefore the ability to control the morphology of γ-AlOOH *via* a green synthesis route has high industrial significance. In itself, γ-AlOOH is a very stable room temperature wide bandgap material.[14] This compound is layered and has been shown to play an important technological role in applications in medicine, composites, catalysis, ceramics, electronics and other technologies.[12c, 15] In addition γ-AlOOH is potentially a strong candidate for filtering applications.[15c, 16] Layered oxide-hydroxides of aluminum feature various properties such as room temperature stability and high mechanical stiffness.[14] Nanostructures of γ-AlOOH, that offer high surface area, have been developed using a variety of liquid phase techniques[13b, 17] However, methods of producing γ-AlOOH with large surface area involve complex synthesis processes with narrow windows to control the growth morphology. They are generally power intensive, require high temperatures, extensive processing times, or usage and/or release of toxic chemicals.

Here we present a green liquid metal based technique for synthesizing 1D and 2D γ-AlOOH structures grown from the surface of galinstan at the interface with H_2O. The 1D fibers and 2D sheets grow perpendicular and parallel to the surface of the liquid galinstan, respectively, with large surface areas. The 1D and 2D morphologies of γ-AlOOH are retained when converted into γ-Al_2O_3 *via* annealing. Quantitative nanomechanical mapping (QNM) indicated that the 2D γ-AlOOH sheets feature the highest Young's modulus among oxides.[18] Free-standing membranes are successfully

constructed consisting of layered 2D sheets of AlOOH for separating oil-in-water emulsions and filtering Pb^{2+} ion contaminated water. Importantly, the synthesis of naturally forming free standing membranes does not require a template, structural support, compression or sintering due to the high degree of stiffness of the structure. These membranes, which operate at extraordinary flux rates, can reduce Pb^{+2} ion contamination at a concentration that is >13 times above standard drinking water to safe levels. After completion of the nanomaterial synthesis, the galinstan can be reused for the next synthesis cycle providing a sustainable, green and low cost process. We clearly demonstrate that after three cycles of synthesis using the same liquid metal that the quality of the products does not degrade with negligible consumption of the liquid metal. The synthesis provides a simple method for obtaining close to 100% production yield with only the need for aluminum and water as precursors and without the participation of any toxic solvents.

2. Results and Discussion

Galinstan is prepared using a thermal alloying protocol[2b] presented in Experimental section. Aluminum containing alloys are prepared using a mechanical alloying procedure adopted from the literature (see Experimental section).[2b] The prepared aluminum alloys are then exposed to aqueous environments. **Figure 1** a and b show schematically the synthesis protocol in the liquid (water) and gas (vapor) phases, respectively. During the synthesis using liquid water, the galinstan-aluminum alloy, with an optimum ~3.3 wt% Al (the highest surface area of the product is obtained at this concentration which will be discussed later), which is still in droplet form is placed inside a glass vial with deionized (DI) water (Figure 1a). The reaction is immediate and the product from this synthesis

is a hydrogel as shown in the photo in Figure 1a (see Experimental section for details). The growth mechanism is illustrated in Figure 1a in which bubbles start to form on the liquid metal surface, exfoliating the 2D sheets at the surface into the DI water. Figure 1b shows the synthesis schematic using water vapor. In this approach a glass vial containing the galinstan-aluminum droplet is exposed to water vapor (see Experimental section for details). The product from this synthesis method features an aerogel as shown in the associated photo in Figure 1b. The growth mechanism is also illustrated in Figure 1b in which 1D structures grow perpendicular to the surface of the liquid metal. Under these conditions water vapor nucleation occurs on the surface of the liquid metal, creating small sites in which fibrous structures grow (Figure 1b and **Figure S1**). In a similar manner chemical vapor deposition (CVD) is also known to produce well aligned 1D structures grown from catalytic nanoisland.[19] These structures do not delaminate from the surface of the liquid metal but grow continuously upward as shown in the images. Contact angle measurements of water droplets are presented in **Figure S2a** which show surface of pristine galinstan liquid metal is relatively hydrophilic with contact angle of 4.4 ± 0.1 º. During water-based synthesis, galinstan-aluminum alloy does not sustain a water droplet (Figure S2b). During the vapor-based synthesis, the surface of galinstan-aluminum alloy is covered with micron or submicron diameter water droplets that form the 1D structure seeds (Figure S2c). After the completion of both methods of synthesis, when the hydrogel and aerogel are removed from the galinstan droplet, the latter remains unchanged. This indicates that in principle the galinstan can be reused for the next synthesis cycle (Figure 1c). This reusability is explored (which will be discussed later) and presented in the Experimental section.

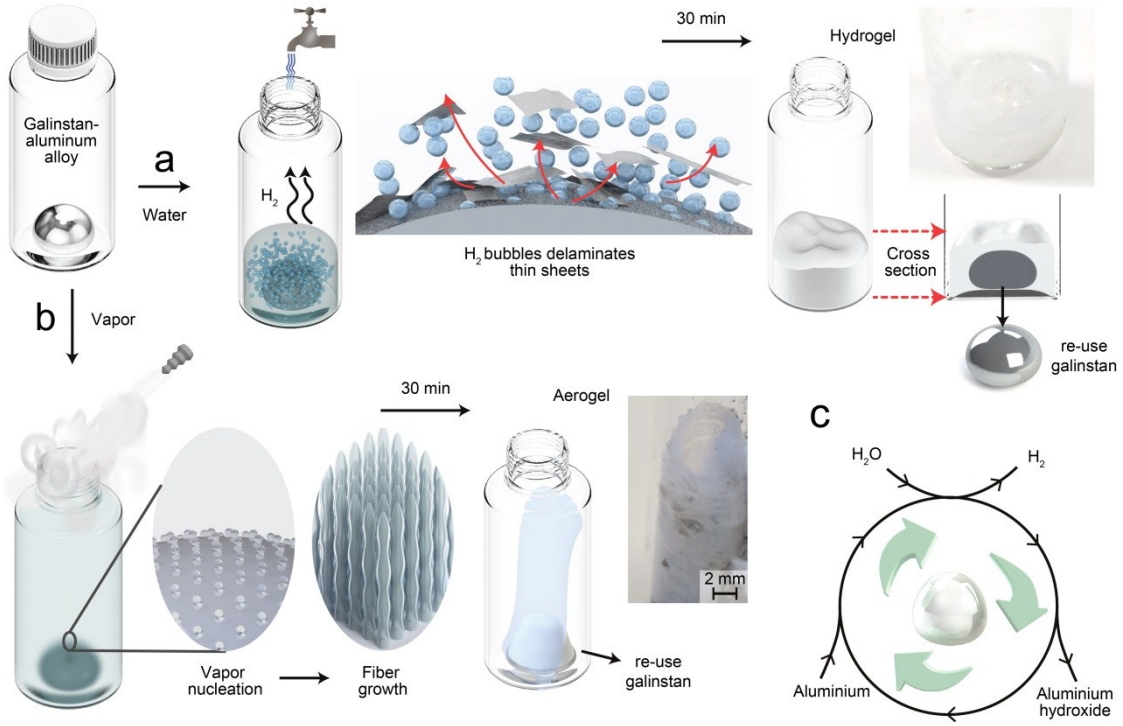

Figure 1. (**a**) DI water is added to a drop of a liquid metal alloy of galinstan-Al. After 30 min of exposure to water a hydrogel is formed. The proposed growth mechanism of the product shows that the skin is delaminated by hydrogen bubbles in the form of sheets into the DI water. The photo shows the final product from adding 2 ml DI water to 0.5 g of a 3.3 wt% galinstan-Al alloy. (**b**) Vapor is fed into the glass vial containing 0.5 g of 3.3 wt% galinstan-Al. After 30 min an aerogel has grown from the liquid metal. The growth mechanism shows the emergence of fibrous structures from the vapor nucleation sites. The photo shows the aerogel that has grown from the surface of the liquid metal. (**c**) The reaction stops after the consumption of all the aluminum but the galinstan remains unchanged after producing the aluminum hydroxides. Therefore, a green process is adopted to reuse the galinstan for the next synthesis cycle.

Transmission electron microscopy (TEM), scanning electron microscopy (SEM) and atomic force microscopy (AFM) images show that exposure to liquid and vapor phases produce 2D sheets (**Figure 2**a-c) and 1D fibers (Figure 2g-i), respectively. AFM images in Figure 2c and 2j present the nominal thicknesses of 2D sheets and 1D fibers to be ~1.2 and ~2.3 nm, respectively (Figure 2c and i). The 2D sheets and 1D fibers feature large lateral dimensions with their lengths extending tens of micrometers. High resolution TEM images together with selected area electron diffraction (SAED) and X-ray diffraction (XRD) patterns (Figure 2d, e, j and k) indicate a match for the orthorhombic phase (γ-phase) of AlOOH with lattice spacings of a = 3.700 Å, b = 12.227 Å and c = 2.868 Å (space group *cmcm*, no. 63). Both 2D and 1D γ-AlOOH feature polycrystalline and poorly crystalline structures, respectively. Poorly crystalline boehmite is sometimes referred to as pseudo-boehmite.[20] However, for consistency we use the term boehmite or γ-AlOOH in this work. The Raman spectrum of the 2D sheets (Figure 2f) shows more defined peaks than that of the 1D fibers of γ-AlOOH (Figure 2l), due to the stronger crystallinity of the sheets.[21]

Since boehmite (γ-AlOOH) is a layered material[22], unit cell thick 2D sheets for TEM and AFM analysis were obtained by diluting samples to 10 mg/L with DI water and sonicating for 5 minutes. The 2D sheets thickness histogram with a peak around a unit cell is shown in Figure S3. Synthesized nanofiber morphologies are sonicated using an identical procedure to that of sheets. No change in thickness of the exfoliated nanofibers is observed with modifying the amount of alloyed aluminum, used water or the steam temperature variations from 100 to 200 ºC. Equation (1)[15c] describes the

hydrogel formation process. The obtained hydrogel is composed of a two-phase colloidal system[23] containing water and α-$Al(OH)_3$ (bayerite). The presence of bayerite confirmed through Raman spectroscopy (**Figure S4**) which itself is a layered material.[24] The sample is then converted to γ-AlOOH following Equation (2)[10a, 25] at 170ºC (see Experimental section). Equation (3) represents a single step growth of 1D γ-AlOOH aerogels using the vapor synthesis route.[26]

$$2Al + 6H_2O \rightarrow 2Al(OH)_3 + 3H_2 \quad (1)$$

$$Al(OH)_3 \rightarrow AlOOH + H_2O \quad (2)$$

$$2Al + 4H_2O \rightarrow 2AlOOH + 3H_2 \quad (3)$$

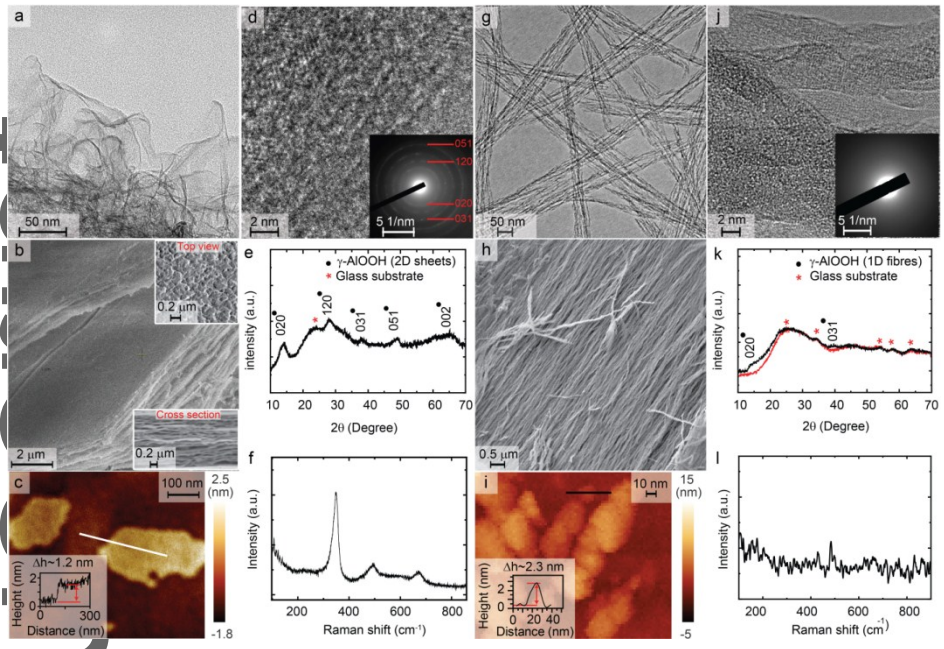

Figure 2. Characterization (a-g) of 2D and (**h-m**) 1D γ-AlOOH (**a-c**) TEM, SEM and AFM images of 2D sheets that are as obtained products of water-based synthesis dried at 170°C. (**e-g**) HRTEM with SAED (inset), XRD and Raman spectroscopy, respectively, show that the dried 2D sheets are γ-AlOOH.[21] (**h-j**) TEM, SEM and AFM images of the obtained products from vapor-based synthesis that include 1D fibers. (**k-m**) HRTEM with SAED (inset), XRD and Raman spectroscopy, respectively, clearly show that the 1D fibers are poorly crystalline γ-AlOOH.

Boehmite is the main precursor for the synthesis of γ-Al_2O_3 as described in Equation (4),[10a, 27] where after being annealed at ~550ºC boehmite converts to γ-Al_2O_3.[10a] HRTEM, XRD (**Figure 3**) confirm the conversion to the γ phase and the crystal morphology matches the cubic phase. Interestingly, low resolution TEM images (Figure 3 a and d) reveal that the 2D and 1D nature of the initial γ-AlOOH is retained even after the high temperature conversion to γ-Al_2O_3. HRTEM images indicate that both

2D and 1D γ-Al_2O_3 feature polycrystalline domains (Figure 3 b and e are selected to show the crystalline sections). Also, XRD of the 1D γ-Al_2O_3 sample shows sharper peaks than that of its 2D counterpart, whereby 1D γ-Al_2O_3 also presents additional [111] and [333] peaks. The 1D material is randomly oriented leading to a more complete powder pattern in comparison to the 2D material that is highly oriented leading to the missing peaks.

$$2\ AlOOH \rightarrow Al_2O_3 + H_2O \qquad (4)$$

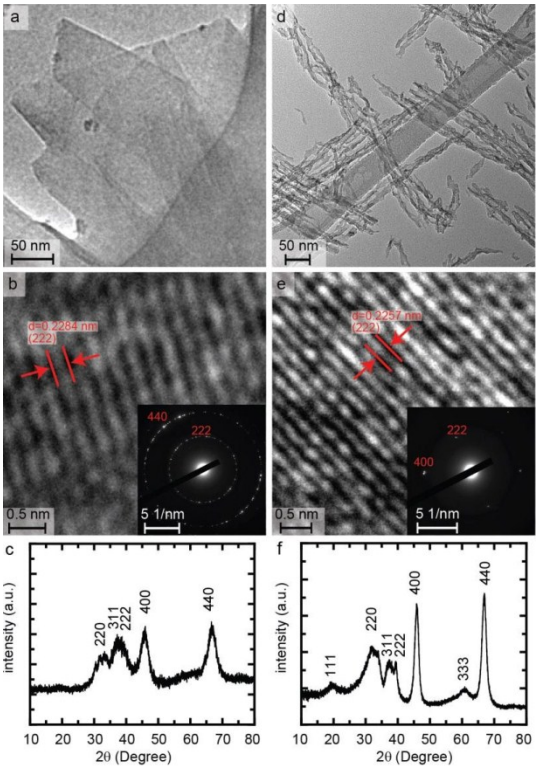

Figure 3. Characterization of annealed γ-Al_2O_3. Left and right columns present 2D and 1D γ-Al_2O_3 respectively. (**a** and **d**) low resolution TEM images and (**b** and **e**) high resolution TEM images of a selected crystalline section. (**c** and **f**) show the associated XRD patterns.

Peak force quantitative nanomechanical mapping (PF-QNM) is a high-resolution AFM based technique that allows determining the Young's modulus using the Derjaguin–Mueller–Toporov (DMT) model.[28] Additional information regarding this technique can be found in the Experimental section. The 2D sheet's Young's modulus of γ-AlOOH and γ-Al_2O_3 are found to be 495.7 and 96.2 GPa, respectively (**Figure 4** a and b). The Young's modulus map of the 2D γ-AlOOH indicates that the as synthesized boehmite sheets are a stiffer material than the subsequently synthesized γ-Al_2O_3. A wide range of Young's modulus distribution are measured for γ-AlOOH (Figure 4a) which may be due to its highly wrinkled 2D structure.

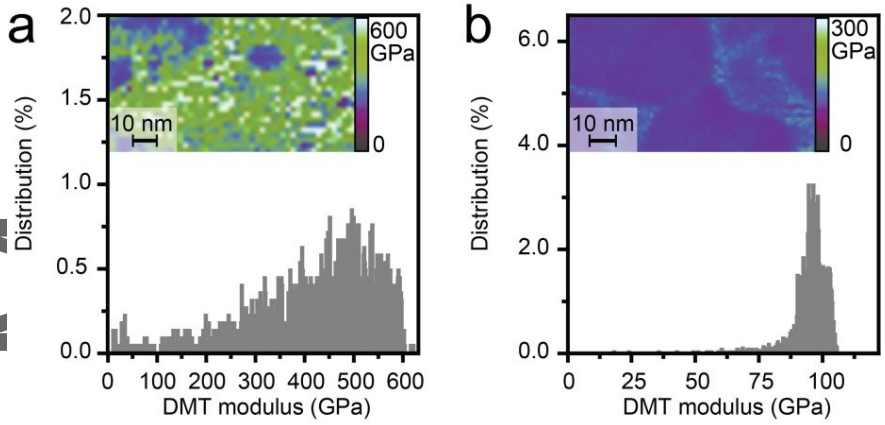

Figure 4. (**a** and **b**) Peak force quantitative nanomechanical mapping (PF-QNM) AFM characterization of 2D γ-AlOOH and 2D γ-Al_2O_3 flakes, respectively. Corresponding DMT modulus maps are shown above the histogram.

High surface area γ-AlOOH and Al_2O_3 species are of tremendous technological significance due to the wide spread use of these compounds as catalyst support, polymer fillers and ion exchange filters, are increased surface areas correlate with superior performance.[15c, 16, 29] Therefore the developed synthesis route for 2D γ-AlOOH is optimized towards increased surface areas. The surface area of the final product is found to depend on the alloyed concentration of aluminum as presented in **Figure 5**a. A substantial enhanced surface area is observed for alloys containing above 2.5 wt% of Al and the optimized alloy concentration is identified to contain ~3.3 wt% of aluminum. The overall synthesis yield for the 2D γ-AlOOH product can be increased by increasing the concentration of aluminum as demonstrated in **Figure S5**. However, at high concentrations some bayerite somatoids are also formed (**Figure S6**).

The optimized alloy for producing 2D γ-AlOOH is selected for the synthesis of 1D γ-AlOOH and correspondingly annealed to 1D and 2D γ-Al_2O_3. The 1D and 2D structures of γ-AlOOH have maximum measured surface areas of 906 and 654 m^2g^{-1}, respectively (Figure 5a, see **Figure S7** for the corresponding N_2 adsorption and desorption isotherms). After annealing, the surface areas of the 1D and 2D γ-Al_2O_3 are reduced to 418 and 396 m^2g^{-1} respectively.

The recyclability of the used galinstan is of significant importance, due to the comparatively high retail price of indium and gallium. It is observed that upon the completion of the γ-AlOOH synthesis, the liquid metal solvent is found to be well separated from the product, which suggests that the liquid metal may potentially be simply reused for further reactions, provided that fresh aluminum is alloyed into the melt. Figure 5b shows the surface area data for three cycles of synthesis in which galinstan is reused (schematic is shown in Figure 1c). Both the second and third syntheses cycles show an increased surface area compared to the first synthesis cycle. Gravimetric analysis revealed

that ~3.2 % of the initial galinstan alloy is lost during the three synthesis cycles, with the lost liquid metal being associated with manual handling during transfer steps rather than incorporation into the product or dissolution. Energy dispersive X-ray spectroscopy (EDXS) results shown in Figure 5c indicate that the obtained product has no metal inclusions. This is achieved after a slow centrifugation step at 50 RCF for a period of 15 min which effectively removes any metal droplets. On the other hand, Figure 5d shows no aluminum on the surface of the liquid metal after three synthesis cycles, indicating complete conversion of the metallic Al into aluminum oxides and oxide hydroxides and a synthetic yield of close to 100 %. The EDXS spectra corresponding to Figure 5 c and d are shown in **Figure S8 and S9**, respectively.

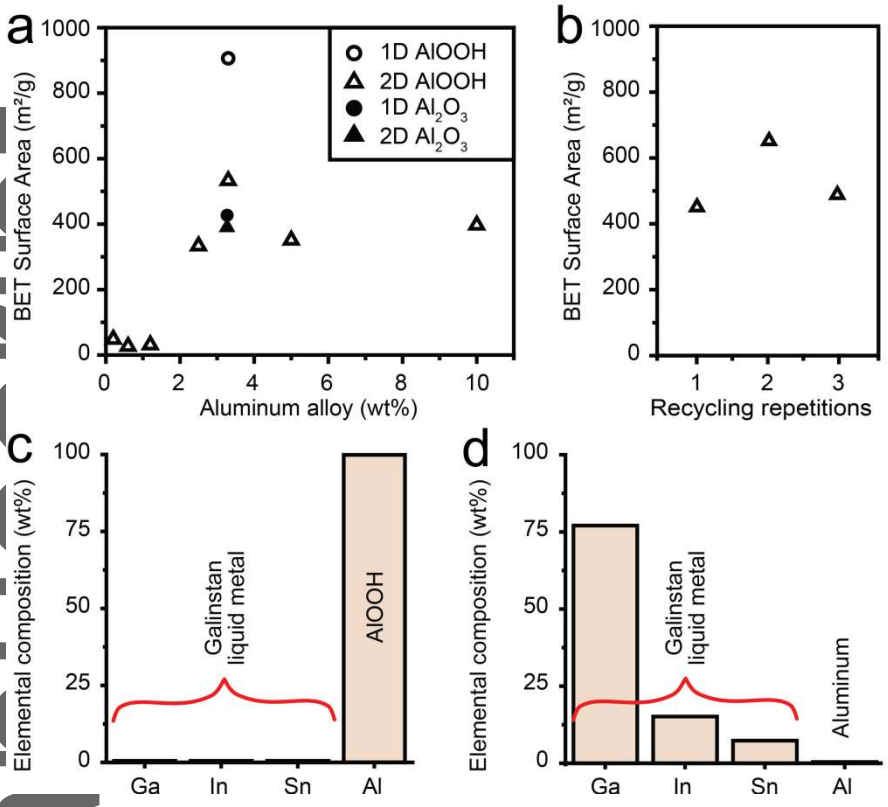

Figure 5. (**a**) Optimization of the BET of surface area of the 2D γ-AlOOH by changing the aluminum concentration. (**b**) Green synthesis shown in Figure 1c with three repetitions showing an increase in surface area after two repetitions. (**c**) EDXS elemental composition results for the low centrifuged products demonstrate no metal inclusions and (**d**) no aluminum is found on the surface of the liquid metal after completion of three synthesis cycles.

In addition to possessing a wide band gap, high surface area, excellent mechanical stiffness and room temperature stability,[8, 14] γ-AlOOH features further unique properties that may lead to potential industrial applications. **Figure 6**a shows 1D γ-AlOOH aerogel structure that is grown on the surface of a galinstan droplet. The grown sample is evidently mechanically staple and capable to

support its own weight. The transparency to visible-light is due to the wide bandgap of boehmite and attests the absence of liquid metal inclusions.

γ-AlOOH is widely used in membrane applications due its ability to adsorb heavy metal ions (including Cr^{3+},Pb^{2+}, Zn^{2+}, Cd^{2+}, Co^{2+}, Hg^{2+}),[15c, 16a-c] sulphate[16d] and phosphates.[15c, 16b-f] Figure 6b illustrates the approach to fabricate free-standing membranes from delaminated self-assembled 2D sheets of γ-AlOOH. A typical membrane has a thickness of ~28.7 µm. (Figure 6 b and c). Details of membrane preparation are presented in the Experimental section. High adsorption capacities and kinetics of Pb^{2+} ions by nanostructures of γ-ALOOH and its incorporated membranes have been reported.[16a, 16e, 30] To test the membrane's performance, lead ions are chosen as a water pollutant. A ~200 ppb solution containing Pb^{2+} ions (> 13 times above the permitted level of standard drinking water)[31] is prepared and passed through the membrane. Inductively coupled plasma mass spectrometer (ICP-MS) measurements show that the initial ~200 ppb concentration of Pb^{2+} is reduced to ~2 ppb, thereby removing 99 % of lead ions from the water and reducing the contaminant concentration to a safe drinking level (Figure 6c).[31] The schematic of this process is shown in Figure 6d.

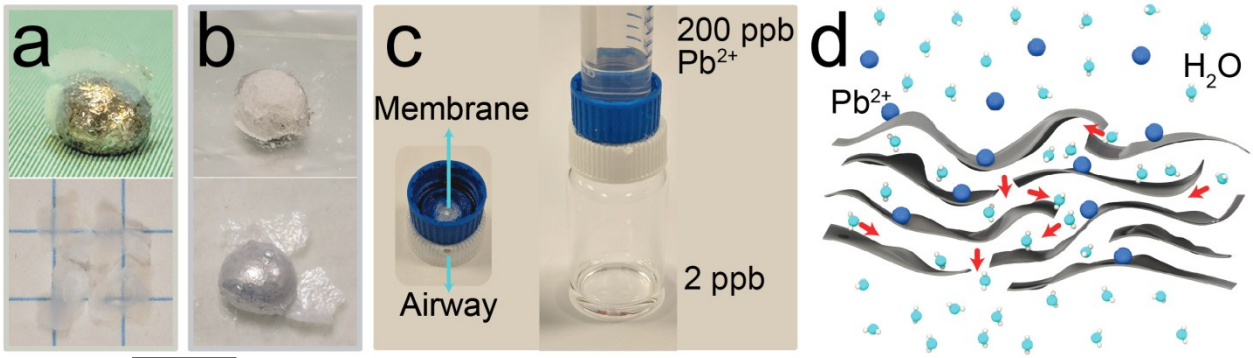

Figure 6. (**a**) Vapor grown and (**b**) water grown γ-AlOOH self-assembled structures, respectively. As shown in **a**, self-assembled structures grown on a galinstan droplet form 1D fibers of γ-AlOOH which result in a translucent material. The photo on the bottom of **a** demonstrates the transparency of the material on graph paper with 5×5 mm grid sizes. **b** shows the grown and delaminated layers of self-assembled 2D structures of γ-AlOOH. Synthesis process is detailed in the Experimental section. (c) photos of an experiment and a fabricated membrane are presented on the right and the left side, respectively. (**c**) schematic of the membrane adsorption of lead ions during filtration is shown.

The membrane is then tested for oil/water separation for a ~40:60 %wt:wt oil-in-water emulsion as (**Figure 7**a). Thermal gravimetric analysis (TGA) analysis of the permeate and retentate (Figure 7b) reveals that the developed membrane achieved a 98.5 % rejection rate of oil. Schematic of the oil/water seperation is presented in Figure 7c. Final concentrations of permeate and retentate contain ~99.3 wt% water and ~97.2 wt% oil, respectively. Both membranes are gravity driven with water fluxes exceeding 8.4×10^4 $Lm^{-2}h^{-1}bar^{-1}$. The excellent pollutant removal capabilities combined with the ease of membrane fabrication highlight the potential of the developed materials for water purification applications. Furthermore, the straightforward synthesis of the nanomaterials with

minimal reaction workup and quantitative yield, combined with the direct reusability of the liquid metal, render the process to be highly attractive.

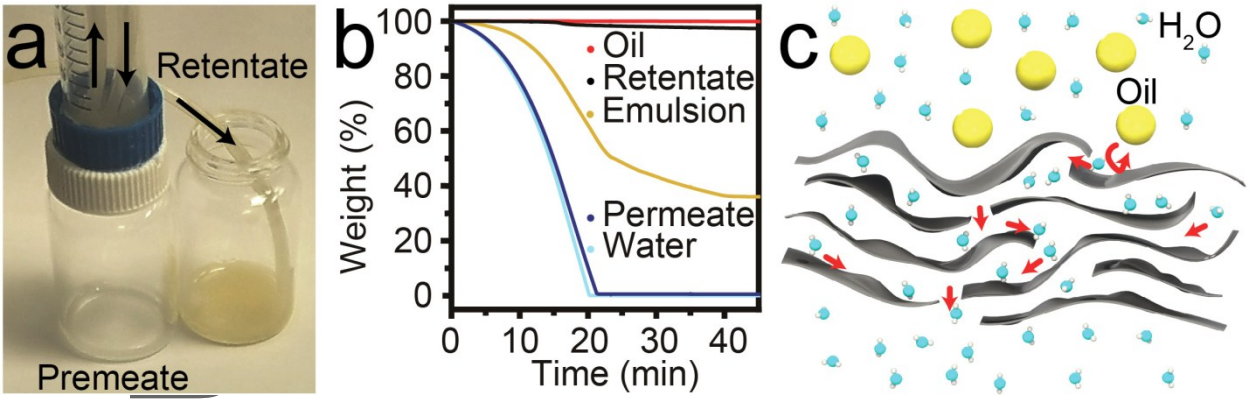

Figure 7. (**a**) The photo shows the experimental setup in which the arrows indicate the direction of the flow to/from a multi-channel peristaltic pump. (**b**) TGA analysis of the oil-in-water emulsion separation performance of the membrane**.** (**c**) Schematic of oil-in-water emulsion separation in which water permeates through the membrane however and oil is retained.

Thermodynamic considerations dictate the reaction and composition at the interface of the gallium liquid metal alloy with an oxygen environment when mixed with different metals.[2b] When aluminum is alloyed into galinstan, and the melt is kept in an oxidizing environment, an oxide of aluminum is preferentially formed on the surface of the liquid metal. The emergence of aluminum oxide on the surface is associated to its lower Gibbs free energy of formation in comparison to gallium, indium and tin oxides.[2b] Here, the liquid metal is interfaced in an aqueous environment instead of an oxygen containing atmosphere to produce hydroxide and oxide hydroxide of

aluminum. The synthesis requires aluminum and water as the only precursors, with the liquid metal solvent being directly reusable for multiple batches without the need for any purification steps. The synthesized low dimensional γ-AlOOH can be converted to γ-Al_2O_3 by annealing while allowing to retain the morphology of the synthesized structures.

The γ-AlOOH materials feature interesting chemical, optical and mechanical characteristics. Both 1D and 2D γ-AlOOH have high surface areas, while the former is capable of forming highly translucent aerogels, the latter is extremely stiff. The synthesized 2D γ-AlOOH featured an excellent average surface area of ~532 m^2/g for multiple synthesized batches, and mechanical stiffness of ~495.7 GPa, the highest ever reported amongst all studied 2D oxide compounds.

In addition to high surface area and mechanical stiffness, γ-AlOOH also features a layered crystal structure,[20] and ionic adsorption properties.[15c, 16] The synthesized 2D γ-AlOOH sheets could be directly utilized for water decontamination applications and demonstrated to enable high performance heavy metal ion (>99% lead ion collection) and oil removal from water (>98.5% oil content separation). When compared with other 2D material based decontamination membranes, the developed 2D γ-AlOOH based membranes are capable to support a much higher water flux (>8.4×10^4 $Lm^{-2}h^{-1}bar^{-1}$) (ion filtration) when compared to the highest reported flux of many other layered materials such as MXene, MoS_2, WS_2 and GO, with water fluxes of 6×10^3, 243, 730 and 71 $Lm^{-2}h^{-1}bar^{-1}$, respectively.[32] The extraordinarily high flux is possibility due to disordered boehmite sheets that are highly wrinkled and allow large openings for water molecules to permeate. Figure S7a shows the pore width obtained from BET analysis which suggests pore sizes between 3-20 nm.

It has been shown that GO membranes ion adsorption is significantly improved when combined with alumina.[29c, 29d, 33] For γ-AlOOH has been suggested to be due to an ion exchange mechanism as reported for phosphates[16f], formation of layered double hydroxides (LDH) with divalent metal cations,[34] or electrostatic attraction to the hydroxyl (OH) groups on the surface for the adsorption of ions.[15c, 16b-d]

3. Conclusions:

Using gallium liquid metal as a reaction environment offers a green and low cost synthesis approach for 1D and 2D structures of γ-AlOOH. In brief, we have demonstrated a green and sustainable synthesis process for producing 1D and 2D structures of boehmite that can be annealed into alumina while maintaining their structural integrity. The 2D sheets are remarkably as small as one unit cell of boehmite crystal, giving the material very high surface area. The Young's modulus of the 2D sheets is very large, resulting in the highest reported mechanical stiffness for 2D oxide sheets to date.[18] Membranes are produced that are able to support extraordinary fluxes for the successful separation of heavy metals and oil from water, as a result of high surface area and the wrinkled nature of the 2D sheets.

Altogether, the liquid metal reaction medium enabled the development of a facile process with close to 100 % quantitative yields for synthesizing low dimensional aluminum oxide compounds. The technique is potentially of significant industrial value, since it can be readily up-scaled, the liquid metal can be re-used, and the process requires very short reaction times and proceeds at low temperatures.

4. Experimental Section

Alloy preparation: Galinstan is used as a base liquid metal for dissolving and alloying aluminum. Galinstan is prepared in house by melting 68.5 wt% gallium 21.5 wt% indium and 10 wt% tin in a glass beaker following previously published proceedures.[2b] The precursor materials for galinstan (gallium 99.99%, indium 99.99% and tin 99.9%) are purchased from Roto Metals Inc.

Aluminum wire with diameter 0.58 mm, ≥99.99% purity trace metals basis is procured from Sigma Aldrich. Aluminum is alloyed into the Galinstan *via* grinding using mortar and pestle. The manual grinding process is conducted rigorously for a period of 20 min. Successful alloying is observed when the surface of the alloy became clear and shiny, and the mixture is found to be free from residual metal lumps. The alloying process is conducted inside a N_2 glove box containing <2 ppm oxygen to minimize the oxidization of the alloy. For concentrations exceeding 3.3 wt% aluminum, occasional localized solid lumps are observed.

Liquid water-based synthesis: During the synthesis process (Figure 1a) 0.5 g of the aluminum containing liquid alloy are poured into glass vials inside a N_2 glove box. The alloy is handled inside the nitrogen atmosphere in order to minimize any oxidation that may occur prior to the beginning of the controlled experiment. DI water (2 ml) is rapidly added to the glass vials upon removal from the glovebox. The vial size is chosen to ensure that the added DI water fully covered the surface of the metal droplet, in order to maximize the interfacial reaction region. The reaction is found to immediately begin after the addition of DI water and is completed within approximately 30 min. For further characterization the sample is centrifuged at a low speed of 50 RCF for a period of 15 min to

remove any metal inclusions from the sample. EDXS (Figure S8) confirmed the effective removal of metal inclusions after centrifugation. The sample is then dried via heating at 80 °C. During this step the formed hydrogel transformed from a light grey color to white with a dried appearance. The sample is then heated to 170°C for an additional 4 hours to ensure the full removal of moisture. Under these conditions bayerite is known to transform to boehmite (Equation 1).[49] Further drying at 200 °C for 24 hours is conducted during BET analysis. Boehmite has been found to be stable at this temperature.[9]

Vapor-based synthesis: During this synthesis method (Figure 1b) a glass vial containing 0.5 g of the prepared galinstan-aluminum alloy is prepared inside a flow through N2 glovebox. The glass vial is then placed inside an autoclave. 0.5 ml of DI water is added to the autoclave in the space between the glass vial and the autoclave lining (outside the glass vial containing the alloy). The autoclave packing is conducted inside the flow through glovebox to ensure minimal pre-existing oxidation products. During this process it is imperative to use a continuous flow glove box without oxygen and moisture scrubbers, since the handling of water inside an active glove box may damage the equipment. The DI water is de-gassed prior to use by bubbling nitrogen through the liquid to ensure the removal of any dissolved oxygen. The autoclave is then placed inside an oven and heated to 170°C for 30 min. The autoclave is then allowed to naturally cooled down to room temperature. HRTEM samples are prepared by sonicating a fragment of the isolated material in water for 5 min, followed by drop casting the suspension onto TEM grids.

Repetition, evidencing green synthesis: A 2.5g sample of galinstan is used for this experiment, aluminum is alloyed into the liquid metal via grinding, and the above described synthesis protocol is applied. Following the reaction, the formed oxide species are carefully removed and the liquid metal

droplet is isolated from the bottom of the reaction vial. When each reaction is complete, the products are withdrawn from the liquid metal using a spatula. For the full recovery of the liquid metal, DI water is poured into the glass vial and any left-over hydrogel/aerogel are dispersed into the DI water *via* shaking. The aqueous suspension could then be pipetted out and re-used. The method provided a clean and complete recovery of the liquid metal and products. Visual inspection of the recovered liquid metal indicated the complete removal of the oxides. During the entire experiment care is taken to avoid the loss of any liquid metal. Following the initial synthesis cycle the liquid metal is fully dried, weighed and fresh aluminum is alloyed into the melt for the next reaction cycle. Initial weight of galinstan prior to alloying is measured 2.5 g. After three cycles, the weight of the used droplet is reduced by only 80 mg. A small sample of the liquid metal is smeared onto a Si wafer for SEM based EDXS analysis after the gravimetric analysis. The EDXS analysis revealed the complete removal of aluminum after the third cycle of reusing the liquid metal solvent (Figure 5d and Figure S9).

Membrane preparation: Reaction between liquid metal alloy and DI water is aggressive in the beginning and rapidly generates hydrogen bubbles. The bubbles delaminate the 2D sheets that are formed on the surface of the liquid metal. To produce thin membranes with high integrity structures, liquid metal alloy first is reacted with water for ~20 min to slow down the reaction dynamics. The liquid metal is then separated from hydrogel and is used for membrane preparation. Then surface of the liquid metal is covered with fresh DI water (~0.1 ml). A thin film of hydrogel forms on the surface of the droplet during 5-10 min (Figure 6b photo on top). Then, the drying procedure which is explained in the water-based synthesis of the Experimental section is applied. Drying process transforms hydrogel to a thin film of γ-AlOOH on surface of the liquid metal droplet.

This thin film is then carefully separated from the liquid metal to avoid any metal inclusions and cracks (Figure 6b photo at the bottom). An opening with diameter of ~2 mm is made on caps of a standard laboratory glass vial and a 15 ml centrifuge tube. As seen in Figure 6c, a membrane is made by fixing the thin film of γ-AlOOH together with caps using silicon glue. Cap openings are aligned and the thin film of γ-AlOOH blocks the gap between the caps. All areas around the membrane are sealed using silicon glue. Glue is left to dry for 24 hours. An airway which is shown in Figure 6c is punched on the upper side of the glass vial cap to allow air to exit during the filtration process. Bottom of the centrifuge tube was cut for adding the emulsions and aqueous solutions above the membrane (Figure 6c and Figure 7a).

Emulsion preparation: Oil-in-water (50:50 %v:v) emulsion is prepared by stirring Milli-Q water and semi-synthetic engine oil with the addition of 1 v% surfactant (Tween 80).[35] The emulsion is stirred at 1000 RPM for one hour (IKA stirrer model C-MAG HS4). The emulsion is stirred at lower rates of 250 RPM during experiments. Tween 80 surfactant which has a typical high HLB of 15 is selected to create stable oil-in-water emulsion. Tween 80 boiling point is near 100°C and evaporates with Milli-Q water during TGA analysis.

Annealing for conversion of γ-AlOOH to γ-Al_2O_3: Both 1D and 2D γ-AlOOH are placed on quartz slides and placed inside a thermo scientific thermolyne muffle furnace. They are then heated at 1ºC/min to 550ºC and kept at that temperature for 15 hours. For XRD characterization, 2D γ-Al_2O_3 is ground in a mortar and pestle and hand pressed onto a glass slide, however 1D γ-Al_2O_3 is simply pressed onto the glass slide and the softer nature of the product did not require grinding.

Instrumentation and characterization: A Horiba scientific LabRAM HR evolution Raman spectrometer equipped with a 50× objective lens, a 532 nm laser source (intensity 4.5 mW at the sample position) and a 1800 lines per mm grating is utilized for Raman spectroscopy. Single accumulations spectra with a duration of 200 seconds are collected. The samples are deposited on either gold or glass. Surface topography and high resolution quantitative nanomechanical property mapping (Peak Force QNM) measurements are conducted using a Bruker Dimension Icon AFM. The instrument features a noise floor at less than 30 pm enabling imaging at sub-nanometer resolution. The AFM is equipped with ScanAsyst® Imaging and NanoScope® software 1.8. Tips with less than 5 nm diameters are used for measurements. Peak Force QNM is fully calibrated and software is updated accordingly. Software provides high resolution Young's modulus map of the scanned area using Derjaguin–Mueller–Toporov (DMT) model. We use SiO_2 as substrate. Trenches are cut on the substrate to enable holding flakes in suspended position and avoid contribution of the substrate in measurement. Trenches are made with FEI Scios instrument explained in this section. JEOL 2100F TEM/STEM (2011) operating with 200 keV acceleration voltage is used for most of HRTEM imaging. The instrument is equipped with Gatan Orius SC1000 CCD Camera. For TEM image processing, we use Gatan microscopy suite 1.8.4. Samples are sonicated for 5 min inside DI water to enable drop cast onto a TEM grid. 2D sheets of AlOOH are found to be beam sensitive and the electron beam reduces the crystallinity of the material. High and low resolution SEM is undertaken using a FEI Verios 460L (operating under high vacuum at 1 KV, using stage bias voltages of 1000 to 50 V and through-the-lens low energy electron detector). Patterning of SiO_2 substrates for nanomechanical mapping is performed using an FEI Scios Dual Beam FIB/SEM (focused ion beam/scanning electron microscope) with a Gallium (Ga) beam of 7 nA. Bruker D8 Advance wide angle powder X-Ray

Diffractometer is used to conduct the XRD measurements. All measurements are conducted on glass substrates. Brunauer–Emmett–Teller (BET) is carried out using a Micromeritic ASAP 2000 surface area analyzer to determine surface area with nitrogen gas adsorption. Micro active v2 softwrae which uses Hasley equations is used for data analysis. Samples are degassed under vacuum at 200°C for 24 hours using the instrument. Samples weights are measured before degassing and after degassing. In addition, all samples composition are analyzed by ESDX to correct the weight for any liquid metal inclusions. Agilent ICP-MS with laser ablation capability is used to determine the concentrations of lead ions prior and after filtration. Solutions concentrations are reduced to 1:10 and are prepared to contain 2% HNO_3 before analysis with the instrument. Bruker Contour GT-I 3D optical profiler is used to measure membrane thickness. Optical contact angle is measured using OCA20 instrument from DataPhysics, GmbH. Instrument software interface (CSA20 DataPhysics GmbH), is used for analyzing the contact angles.

Supporting Information

Supporting Information is available from the Wiley Online Library or from the author.

Acknowledgements

Supported by Australian Research Council Centre of Excellence FLEET (CE170100039). We thank the facilities and scientific and technical assistance of the RMIT Microscopy and Microanalysis Facility (RMMF) and the RMIT Micro Nano Research Facility (MNRF). We acknowledge the Ministry of

Science, Technology and Innovation of Brazil (CNPq) that funded Dr. Isabela Alves de Castro (Grant 200698/2015-0).

5. References

[1] a) M. D. Dickey, *ACS Appl. Mater. Interfaces* **2014**, 6, pp. 18369-18379; b) E. J. Markvicka, M. D. Bartlett, X. Huang, C. Majidi, *Nat. Mater.* **2018**, pp. 618–624 ; c) H. Wang, B. Yuan, S. Liang, R. Guo, W. Rao, X. Wang, H. Chang, Y. Ding, J. Liu, L. Wang, *Mater. Horizons* **2018**, 5, pp. 222-229; d) E. Palleau, S. Reece, S. C. Desai, M. E. Smith, M. D. Dickey, *Adv Mater.* **2013**, 25, pp. 1589-1592; e) J. Tang, X. Zhao, J. Li, R. Guo, Y. Zhou, J. Liu, *ACS Appl. Mater. Interfaces* **2017**, 9, pp. 35977-35987; f) N. Kazem, M. D. Bartlett, C. Majidi, *Adv. Mater.* **2018**, 30, 1706594; g) R. A. Bilodeau, D. Y. Zemlyanov, R. K. Kramer, *Adv. Mater. Interfaces* **2017**, 4, 1600913; h) R. K. Kramer, C. Majidi, R. J. Wood, *Adv. Funct. Mater.* **2013**, 23, pp. 5292-5296; i) P. Sen, C. J. Kim, *IEEE Trans. Ind. Electron.* **2009**, 56, pp. 1314-1330; j) A. Zavabeti, T. Daeneke, A. F. Chrimes, A. P. O'Mullane, J. Zhen Ou, A. Mitchell, K. Khoshmanesh, K. Kalantar-zadeh, *Nat. Commun.* **2016**, 7, 12402.

[2] a) B. J. Carey, J. Z. Ou, R. M. Clark, K. J. Berean, A. Zavabeti, A. S. R. Chesman, S. P. Russo, D. W. M. Lau, Z.-Q. Xu, Q. Bao, O. Kavehei, B. C. Gibson, M. D. Dickey, R. B. Kaner, T. Daeneke, K. Kalantar-Zadeh, *Nat. Commun.* **2017**, 8, 14482; b) A. Zavabeti, J. Z. Ou, B. J. Carey, N. Syed, R. Orrell-Trigg, E. L. H. Mayes, C. Xu, O. Kavehei, A. P. O'Mullane, R. B. Kaner, K. Kalantar-Zadeh, T. Daeneke, *Science* **2017**, 358, pp. 332-335.

[3] a) Y. Cui, F. Liang, Z. Yang, S. Xu, X. Zhao, Y. Ding, Z. Lin, J. Liu, *ACS Appl. Mater. Interfaces* **2018**, 10, pp. 9203-9210; b) T. Daeneke, K. Khoshmanesh, N. Mahmood, I. A. de Castro, D. Esrafilzadeh, S. J. Barrow, M. D. Dickey, K. Kalantar-

zadeh, *Chem. Soc. Rev.* **2018**, pp. 4073-4111 ; c) Z. J. Farrell, C. Tabor, *Langmuir* **2018**, 34, pp. 234-240.

[4] T. Y. Liu, P. Sen, C. J. Kim, *J Microelectromech S* **2012**, 21, pp. 443-450.

[5] a) J. Zhang, Y. Yao, L. Sheng, J. Liu, *Adv. Mater.* **2015**, 27, pp. 2648-2655; b) G. Choi, J. T. Ziebarth, J. M. Woodall, R. Kramer, D. Sherman, C. R. Allen, presented at 2010 18th Biennial University/Government/Industry Micro/Nano Symposium, June 28 2010-July 1 2010, **2010**.

[6] a) J. A. Rogers, M. G. Lagally, R. G. Nuzzo, *Nature* **2011**, 477, pp. 45-53; b) G. Fiori, F. Bonaccorso, G. Iannaccone, T. Palacios, D. Neumaier, A. Seabaugh, S. K. Banerjee, L. Colombo, *Nat. Nanotechnol.* **2014**, 9, pp. 768–779 ; c) Z. Sun, A. Martinez, F. Wang, *Nat. Photonics* **2016**, 10, pp. 227–238; d) V. Narasimhan, R. H. Siddique, J. O. Lee, S. Kumar, B. Ndjamen, J. Du, N. Hong, D. Sretavan, H. Choo, *Nat. Nanotechnol.* **2018**, pp. 512–519.

[7] a) A. K. Naskar, J. K. Keum, R. G. Boeman, *Nat. Nanotechnol.* **2016**, 11, pp. 1026-1030; b) X. Zheng, H. Lee, T. H. Weisgraber, M. Shusteff, J. DeOtte, E. B. Duoss, J. D. Kuntz, M. M. Biener, Q. Ge, J. A. Jackson, S. O. Kucheyev, N. X. Fang, C. M. Spadaccini, *Science* **2014**, 344, pp.1373-1377; c) J. W. Colson, W. R. Dichtel, *Nat. Chem.* **2013**, 5, pp. 453–465; d) P. Kissel, R. Erni, W. B. Schweizer, M. D. Rossell, B. T. King, T. Bauer, S. Götzinger, A. D. Schlüter, J. Sakamoto, *Nat. Chem.* **2012**, 4, pp. 287–291; e) R. Betancur, P. Romero-Gomez, A. Martinez-Otero, X. Elias, M. Maymó, J. Martorell, *Nat. Photonics* **2013**, 7, pp. 995-1000.

[8] S. S. Singh, *Can. J. Soil Sci.* **1982**, 62, pp. 327-332.

[9] M. F. Peintinger, M. J. Kratz, T. Bredow, *J Mater Chem A* **2014**, 2, pp. 13143-13158.

[10] a) T. E. Bell, J. M. Gonzalez-Carballo, R. P. Tooze, L. Torrente-Murciano, *J Mater Chem A* **2015**, 3, pp. 6196-6201; b) Y. Deng, Q. Yang, G. Lu, W. Hu, *Ceram. Int.* **2010**, 36, pp. 1773-1777.

[11] X. Krokidis, P. Raybaud, A.-E. Gobichon, B. Rebours, P. Euzen, H. Toulhoat, *J. Phys. Chem. B* **2001**, 105, pp. 5121-5130.

[12] a) S. Liu, C. Chen, Q. Liu, Y. Zhuo, D. Yuan, Z. Dai, J. Bao, *RSC Adv.* **2015**, 5, pp. 71728-71734; b) Z. Zhang, T. J. Pinnavaia, *J. Am. Chem. Soc.* **2002**, 124, pp. 12294-12301; c) S. Shen, W. K. Ng, L. S. O. Chia, Y. Dong, R. B. H. Tan, *Cryst. Growth Des.* **2012**, 12, pp. 4987-4994.

[13] a) S. Lamouri, M. Hamidouche, N. Bouaouadja, H. Belhouchet, V. Garnier, G. Fantozzi, J. F. Trelkat, *Boletín de la Sociedad Española de Cerámica y Vidrio* **2017**, 56, pp. 47-54; b) X. Zhang, M. Honkanen, E. Levänen, T. Mäntylä, *J. Cryst. Growth* **2008**, 310, pp. 3674-3679.

[14] X. Zhou, J. Zhang, Y. Ma, H. Tian, Y. Wang, Y. Li, L. Jiang, Q. Cui, *RSC Adv.* **2017**, 7, pp. 4904-4911.

[15] a) B. Sun, Z. Ji, Y.-P. Liao, M. Wang, X. Wang, J. Dong, C. H. Chang, R. Li, H. Zhang, A. E. Nel, T. Xia, *ACS Nano* **2013**, 7, pp. 10834-10849; b) A. Martínez, G. Prieto, J. Rollán, *J. Catal.* **2009**, 263, pp. 292-305; c) C. Gao, X.-Y. Yu, R.-X. Xu, J.-H. Liu, X.-J. Huang, *ACS Appl. Mater. Interfaces* **2012**, 4, pp. 4672-4682.

[16] a) Y. Wei, R. Yang, Y.-X. Zhang, L. Wang, J.-H. Liu, X.-J. Huang, *Chem. Commun.* **2011**, 47, pp. 11062-11064; b) M. Salem, H. Sharawy, M. Ossman, *Kinetics modeling and Adsorption isotherm studies for Cr(III) removal using Boehmite Nano-powder*, **2013**; c) G. Hota, B. R. Kumar, W. J. N. S. Ramakrishna, *J Mater Sci* **2008**, 43, pp. 212-217; d) T. He, L. Xiang, S. Zhu, *Langmuir* **2008**, 24, pp. 8284-8289; e) Y.-X. Zhang, X.-Y. Yu, Z. Jin, Y. Jia, W.-H. Xu, T. Luo, B.-J. Zhu, J.-H. Liu, X.-J. Huang, *J. Mater. Chem.* **2011**, 21, pp. 16550-16557; f) W. P. Tang, O. Shima, A. Ookubo, K. Ooi, *J. Pharm. Sci.* **1997**, 86, pp. 230-235.

[17] a) C. Márquez- Alvarez, N. Žilková, J. Pérez- Pariente, J. Čejka, *Cataly. Rev.* **2008**, 50, pp. 222-286; b) T. F. Baumann, A. E. Gash, S. C. Chinn, A. M. Sawvel, R. S. Maxwell, J. H. Satcher, *Chem. Mater.* **2005**, 17, pp. 395-401; c) C. Xiang Ying, H. Hyun Sue, W. L. Soon, *Nanotechnology* **2007**, 18, 285608; d) T. E. Bell, J. M. Gonzalez-Carballo, R. P. Tooze, L. Torrente-Murciano, *RSC Adv.* **2017**, 7, pp. 22369-22377; e) Z. Gan, G. Ning, Y. Lin, Y. Cong, *Mater. Lett.* **2007**, 61, pp. 3758-3761; f)

A. I. Osman, J. K. Abu-Dahrieh, M. McLaren, F. Laffir, P. Nockemann, D. Rooney, *Sci. Rep.* **2017**, 7, 3593.

[18] a) I. A. Ibrahim, F. A. Mohamed, E. J. Lavernia, *J Mater Sci* **1991**, 26, pp. 1137-1156; b) J. R. Nicholls, D. J. Hall, P. F. Tortorelli, *Mater. High Temp.* **1994**, 12, pp. 141-150.

[19] J. J. Wu, S. C. Liu, *Adv Mater.* **2002**, 14, pp. 215-218.

[20] S. Iijima, T. Yumura, Z. Liu, *Proc. Natl. Acad. Sci. U.S.A.* **2016**, 113, pp. 11759-11764.

[21] R. H. D., F. R. L., K. J. T., *J. Raman Spectrosc.* **2001**, 32, pp. 745-750.

[22] M. F. Peintinger, M. J. Kratz, T. Bredow, *J. Mater. Chem. A* **2014**, 2, 13143-13158.

[23] K. Wefers, C. Misra, *Oxides and hydroxides of aluminum*, Alcola laboratories, **1987**.

[24] M. Digne, P. Sautet, P. Raybaud, H. Toulhoat, E. Artacho, *J. Phys. Chem. B* **2002**, 106, pp. 5155-5162.

[25] E. Czech, T. Troczynski, *Int. J. Hydrog. Energy* **2010**, 35, pp. 1029-1037.

[26] C. Wang, J. Ding, G. Zhao, T. Deng, Y. Liu, Y. Lu, *ACS Appl. Mater. Interfaces* **2017**, 9, pp. 9795-9804.

[27] A. Tonejc, A. M. Tonejc, D. Bagović, C. Kosanović, *Mater. Sci. Eng. A.* **1994**, 181-182, pp. 1227-1231.

[28] a) T. J. Young, M. A. Monclus, T. L. Burnett, W. R. Broughton, S. L. Ogin, P. A. Smith, *Meas Sci Technol* **2011**, 22, 125703; b) B. V. Derjaguin, V. M. Muller, Y. P. Toporov, *J. Colloid Interface Sci.* **1975**, 53, pp. 314-326; c) L. Morales-Rivas, A. González-Orive, C. Garcia-Mateo, A. Hernández-Creus, F. G. Caballero, L. Vázquez, *Sci. Rep.* **2015**, 5, 17164.

[29] a) Y. Ku, H.-M. Chiou, *Water Air Soil Pollut.* **2002**, 133, pp. 349-361; b) C. J. C. M. Laurent, H. A. H. Billiet, L. de Galan, *Chromatographia* **1983**, 17, pp. 394-399; c) H. Kang, L. Gongping, L. Yueyun, D. Ziye, S. Jie, J. Wanqin, *Angew. Chem. Int. Ed.* **2014**, 53, pp. 6929-6932; d) K. Xu, B. Feng, C. Zhou, A. Huang, *Chem. Eng. Sci.* **2016**, 146, pp. 159-165; e) L. Yue- Sheng, B. A. J., *J. Am. Ceram. Soc.* **1991**, 74, pp. 219-224; f) S. Wu, T. Braschler, R. Anker, F. Wildhaber, A. Bertsch, J. Brugger, P.

Renaud, *J. Mem. Sci.* **2015**, 477, pp. 151-156; g) A. Yamaguchi, F. Uejo, T. Yoda, T. Uchida, Y. Tanamura, T. Yamashita, N. Teramae, *Nat. Mater.* **2004**, 3, pp. 337-341.

[30] a) Y.-X. Zhang, Y. Jia, Z. Jin, X.-Y. Yu, W.-H. Xu, T. Luo, B.-J. Zhu, J.-H. Liu, X.-J. Huang, *CrystEngComm* **2012**, 14, pp. 3005-3007; b) J. E. Arreola L, *Masters* Autonomous University of Mexico State, International Nuclear Information System, **2013**.

[31] M. Edwards, S. Triantafyllidou, D. Best, *Environ. Sci. Technol.* **2009**, 43, pp. 1618-1623.

[32] a) L. Sun, H. Huang, X. Peng, *Chem. Commun.* **2013**, 49, pp. 10718-10720; b) L. Sun, Y. Ying, H. Huang, Z. Song, Y. Mao, Z. Xu, X. Peng, *ACS Nano* **2014**, 8, pp. 6304-6311; c) C. E. Ren, K. B. Hatzell, M. Alhabeb, Z. Ling, K. A. Mahmoud, Y. Gogotsi, *J. Phys. Chem. Lett.* **2015**, 6, pp. 4026-4031.

[33] R. K. Joshi, P. Carbone, F. C. Wang, V. G. Kravets, Y. Su, I. V. Grigorieva, H. A. Wu, A. K. Geim, R. R. Nair, *Science* **2014**, 343, pp. 752-754.

[34] Q. Wang, D. O'Hare, *Chem. Rev.* **2012**, 112, pp. 4124-4155.

[35] A. K. Kota, G. Kwon, W. Choi, J. M. Mabry, A. Tuteja, *Nat. Commun.* **2012**, 3, 1025.

Liquid metal-based synthesis processes are developed. They offer sustainable, green and rapid pathways for synthesizing low dimensional morphologies of aluminum oxides and oxide hydroxides. Free-standing membrane filters that enable separation of lead ions and oil from aqueous solutions at high flux are made from the two-dimensional morphologies of aluminum oxide hydroxides.

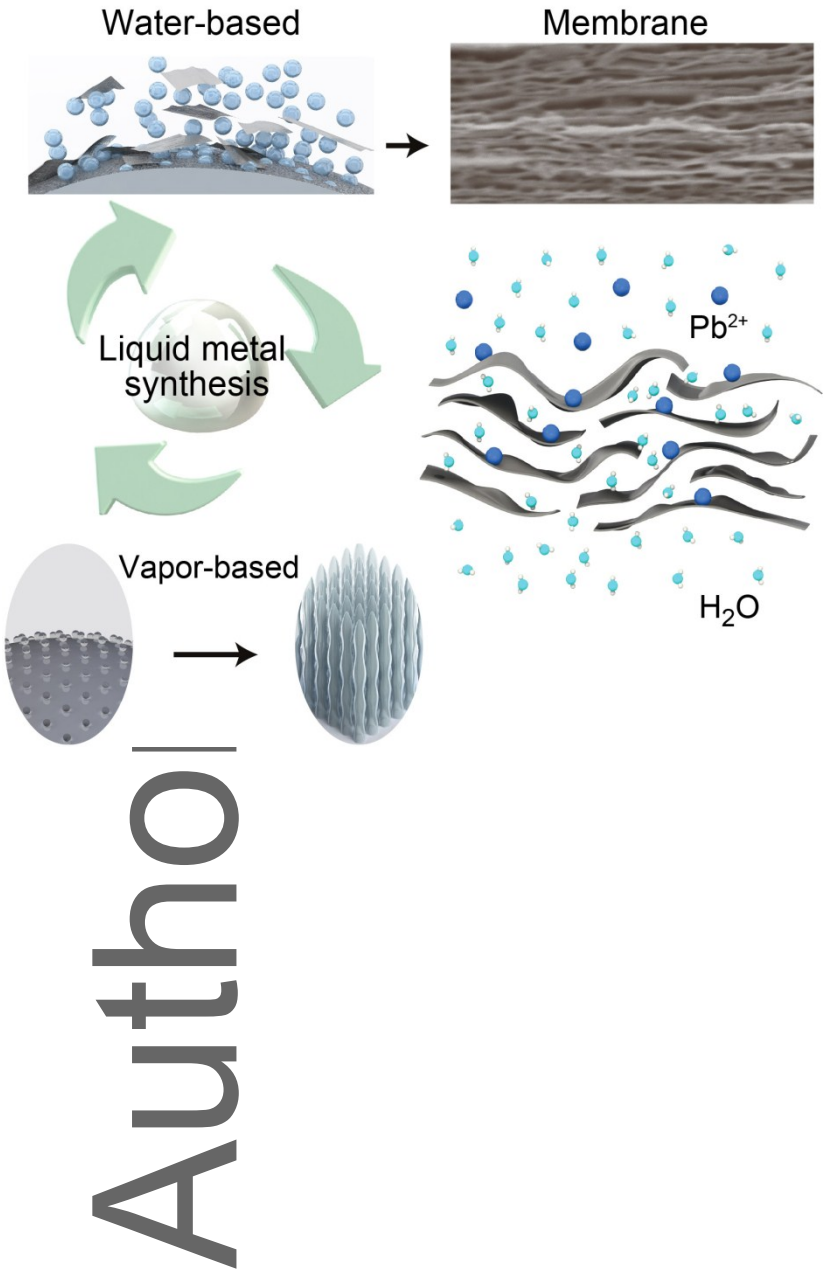

Author/s:
Zavabeti, A;Zhang, BY;de Castro, IA;Ou, JZ;Carey, BJ;Mohiuddin, M;Datta, RS;Xu, C;Mouritz, AP;McConville, CF;O'Mullane, AP;Daeneke, T;Kalantar-Zadeh, K

Title:
Green Synthesis of Low-Dimensional Aluminum Oxide Hydroxide and Oxide Using Liquid Metal Reaction Media: Ultrahigh Flux Membranes

Date:
2018-10-31

Citation:
Zavabeti, A., Zhang, B. Y., de Castro, I. A., Ou, J. Z., Carey, B. J., Mohiuddin, M., Datta, R. S., Xu, C., Mouritz, A. P., McConville, C. F., O'Mullane, A. P., Daeneke, T. & Kalantar-Zadeh, K. (2018). Green Synthesis of Low-Dimensional Aluminum Oxide Hydroxide and Oxide Using Liquid Metal Reaction Media: Ultrahigh Flux Membranes. ADVANCED FUNCTIONAL MATERIALS, 28 (44), https://doi.org/10.1002/adfm.201804057.